Geochemical Perspectives Letters

Experimental evidence for light Ba isotopes favouring aqueous fluids over silicate melts

H. Guo[1,2,3*], W.-Y. Li[4,5*], X. Nan[4], F. Huang[4,5]

doi: 10.7185/geochemlet.2036

Abstract

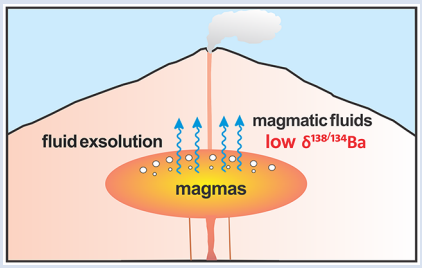

Barium (Ba) is a fluid mobile element and enriched in the Earth's crust, which has potential implications for constraining fluid activities during magmatic-hydrothermal processes. However, the behaviour of Ba and its isotopes during fluid exsolution from magma is poorly known. Here we present an experimental study on determining the Ba partition coefficient ($D_{FLUID\text{-}MELT}$) and equilibrium isotope fractionation factor ($\alpha^{138/134}Ba_{FLUID\text{-}MELT}$) between aqueous fluids and silicate melts with different chemical compositions at 700–900 °C and 200 MPa using cold seal pressure vessels. The results show that $D_{FLUID\text{-}MELT}$ ranges from 0.02 to 0.20, while $\Delta^{138/134}Ba_{FLUID\text{-}MELT}$ [$\approx 1000 \times (\alpha - 1)$] ranges from −0.62 ‰ to −0.14 ‰. Both $D_{FLUID\text{-}MELT}$ and $\Delta^{138/134}Ba_{FLUID\text{-}MELT}$ positively correlate with temperature, the salinity of fluid and alumina saturation index (ASI) of melt. The finding that light Ba isotopes are enriched in aqueous fluids relative to silicate melts suggests that the fluid exsolution process cannot explain the observed light Ba isotopic compositions of some granites. Moreover, the experimentally determined $\alpha^{138/134}Ba_{FLUID\text{-}MELT}$ is useful for tracing fluid activities in felsic intrusion-related hydrothermal deposits and in seafloor hydrothermal systems.

Received 11 July 2020 | Accepted 5 October 2020 | Published 9 November 2020

Introduction

As an alkaline earth metal, Ba is a large ion lithophile element (LILE) and fluid mobile element. It has seven stable isotopes, *i.e.* ^{130}Ba (0.11 %), ^{132}Ba (0.10 %), ^{134}Ba (2.42 %), ^{135}Ba (6.59 %), ^{136}Ba (7.85 %), ^{137}Ba (11.23 %) and ^{138}Ba (71.70 %) (Eugster *et al.*, 1969). Due to the high incompatibility of Ba during mantle melting ($D_{SOLID\text{-}MELT} = 0.00012$; Workman and Hart, 2005), it is strongly enriched in the continental crust relative to the mantle. The average concentration of Ba of the upper continental crust (628 ppm; Rudnick and Gao, 2003) is remarkably higher than that of the average mantle (~7 ppm; Sun and McDonough, 1989). Recently, significant Ba isotopic variations ($\delta^{138/134}$Ba = −0.62 ‰ to +0.15 ‰; Nan *et al.*, 2018) have been observed in granites (Fig. S-1), which may result from assimilation of crustal materials, fractional crystallisation, and/or fluid exsolution. Barium is also strongly enriched in seafloor hydrothermal fluids (1.6 to 100 μmol/kg) compared to seawater (0.14 μmol/kg; Tivey, 2007). The input of Ba from seafloor hydrothermal activities has been suggested to affect the Ba isotopic composition of the deep ocean (Hsieh and Henderson, 2017). Therefore, Ba isotopes may provide a potential tool for constraining differentiation of granitic magma and the oceanic budget of Ba.

Fluid exsolution from melts is common in igneous processes and plays an important role in the formation of magmatic-hydrothermal ore deposits (*e.g.*, Hedenquist and Lowenstern, 1994). Significant stable isotope fractionation of Zn, B and Cu isotopes during fluid exsolution has been demonstrated in previous studies, with corresponding geological applications (*e.g.*, Telus *et al.*, 2012; Maner and London, 2018; Guo *et al.*, 2020). Barium isotopes may also be useful in tracing fluid activities, and the knowledge about the fractionation behaviour of Ba isotopes during magmatic-hydrothermal processes is a necessary prerequisite. However, there is still no study on the key parameter of the equilibrium Ba isotope fractionation factor between aqueous fluids and silicate melts ($\alpha^{138/134}Ba_{FLUID\text{-}MELT}$).

Here, for the first time, we experimentally measured $\alpha^{138/134}Ba_{FLUID\text{-}MELT}$ between aqueous fluids and silicate melts with different chemical compositions at 700–900 °C and 200 MPa. The results show that, in equilibrium, the fluids are isotopically lighter than the melts. This finding promises important applications of Ba isotopes in tracing hydrothermal fluid activities during magma differentiation, magmatic-hydrothermal mineralisation, and seafloor hydrothermal activity.

Methods

Phase equilibrium experiments within cold seal pressure vessels have been widely used to determine the partitioning coefficients of elements (*e.g.*, Borchert *et al.*, 2010). Recently, this method has

1. Bayerisches Geoinstitut, Universität Bayreuth, 95440 Bayreuth, Germany
2. Department of Earth and Planetary Sciences, McGill University, Montreal H3A 0E8, Canada
3. ISTO, UMR 7327 CNRS-Université d'Orléans-BRGM, 45071 Orléans, France
4. CAS Key Laboratory of Crust-Mantle Materials and Environments, School of Earth and Space Sciences, University of Science and Technology of China, Hefei, Anhui 230026, China
5. CAS Center for Excellence in Comparative Planetology, University of Science and Technology of China, Hefei, Anhui 230026, China

* Corresponding authors (email: haihao.guo@cnrs-orleans.fr; wyli@ustc.edu.cn)

been successfully applied to obtain the equilibrium Cu isotope fractionation factors between aqueous fluids and silicate melts (Guo *et al.*, 2020). In this study, similar experiments were performed at 700–900 °C and 200 MPa in rapid quenched cold seal pressure vessels (the capsule design is shown in Fig. S-2a). Besides temperature, chemical compositions of the fluid and melt will also affect the equilibrium Ba isotope fractionation factors, so a series of Ba-doped haplogranitic glasses from peralkaline to peraluminous (with ASI ranging from 0.8 to 1.2), and 0.5–1.5 mol/L NaCl + KCl (Na:K = 1:1 in moles) bearing fluids were used as starting materials. Approximately 1:1 fluid and glass in mass were loaded into gold capsules, and were subsequently equilibrated in the cold seal pressure vessels for 10–40 days. After rapid quenching the experiments, the fluid and glass (quenched melt) phases were carefully and completely separated, and then transferred into solutions respectively. No other mineral phases were observed in the quenched glasses (Fig. S-2b). Afterwards, the Ba concentrations and Ba isotopic compositions of the solutions prepared from the run products were measured by ICP-MS and MC-ICP-MS, respectively. Additional details about the experimental and analytical methods are given in the Supplementary Information.

Results and Discussion

The experimental conditions and results are listed in Table 1. The attainment of equilibrium Ba partitioning and isotope fractionation between fluids and melts was evidenced by the time series experiments. Experiments with the duration of 10, 20 and 40 days show similar results for both $D_{FLUID\text{-}MELT}$ and $\Delta^{138/134}Ba_{FLUID\text{-}MELT}$ (Fig. S-3). In addition, our experimental durations are longer than or comparable to those of previous studies that have achieved equilibrium partitioning of Ba between fluids and melts (*e.g.*, 5–12 days at 750–950 °C and 200 MPa; Borchert *et al.*, 2010). Therefore, the experimental results summarised in Table 1 represent the equilibrium values.

Figure 1 shows that $D_{FLUID\text{-}MELT}$ ranges from 0.02 to 0.20, while $\Delta^{138/134}Ba_{FLUID\text{-}MELT}$ ranges from −0.62 ‰ to −0.14 ‰, both of which change with the temperature and display good positive correlations with salinity of the fluid and ASI of the melt. Specifically, at the fixed melt ASI = 1.0 and fluid salinity of 1 mol/L (Na, K)Cl, $D_{FLUID\text{-}MELT}$ increases from 0.06 to 0.10, and $\Delta^{138/134}Ba_{FLUID\text{-}MELT}$ increases from −0.62 ± 0.07 ‰ to −0.20 ± 0.07 ‰ with temperature increasing from 700 to 900 °C (Table 1, Fig. 1a,b). Both fluid salinity and melt ASI are important factors that affect $D_{FLUID\text{-}MELT}$ and $\Delta^{138/134}Ba_{FLUID\text{-}MELT}$. For example, at 800 °C and the melt ASI of 1.0, increasing the (Na, K)Cl concentration from 0.5 to 1.5 mol/L in the starting fluids enhances $D_{FLUID\text{-}MELT}$ from 0.04 to 0.20, and $\Delta^{138/134}Ba_{FLUID\text{-}MELT}$ from −0.31 ± 0.07 ‰ to −0.14 ± 0.07 ‰, respectively (Table 1, Fig. 1c,d). Similarly, at 800 °C and the fluid with 1 mol/L (Na, K)Cl, increasing the ASI from 0.8 to 1.2 in the starting haplogranitic glasses enhances $D_{FLUID\text{-}MELT}$ from 0.02 to 0.17, and $\Delta^{138/134}Ba_{FLUID\text{-}MELT}$ from −0.44 ± 0.07 ‰ to −0.16 ± 0.07 ‰, respectively (Table 1, Fig. 1e,f).

The correlations of $D_{FLUID\text{-}MELT}$ and $\Delta^{138/134}Ba_{FLUID\text{-}MELT}$ with temperature, fluid salinity and melt ASI can be expressed by numerical regression equations. Since both $D_{FLUID\text{-}MELT}$ and $\Delta^{138/134}Ba_{FLUID\text{-}MELT}$ have a linear function with fluid salinity and melt ASI (Fig. 1c–f), as well as $D_{FLUID\text{-}MELT}$ is generally expressed as a function of 1/T while $\Delta^{138/134}Ba_{FLUID\text{-}MELT}$ as a function of 1/T and $1/T^2$, the regression equations can be described as

$$D_{FLUID\text{-}MELT} = -0.177 \pm 0.159 - (276.0 \pm 151.5) * 1/T + (0.156 \pm 0.027)Cl + (0.373 \pm 0.067)ASI \quad \text{Eq. 1}$$

$$\Delta^{138/134}Ba_{FLUID\text{-}MELT}(‰) = -14.96 \pm 3.32 - (18221013 \pm 4641078) * 1/T^2 + (31828 \pm 8761) * 1/T + (0.167 \pm 0.062)Cl + (0.699 \pm 0.155)ASI \quad \text{Eq. 2}$$

Table 1 Summary of experimental conditions and results.

Run No.	T (°C)	P (kbar)	Duration (days)	Starting melt ASI	Starting fluid	Melt product			Fluid product			D_{Ba}[a]	$\Delta^{138/134}Ba_{FLUID\text{-}MELT}$[b]	2 s.d.[b]
						Ba (ppm)	$\delta^{138/134}Ba$ (‰)	2 s.d.	Ba (ppm)	$\delta^{138/134}Ba$ (‰)	2 s.d.			
Ba05	800	2	10	1.0	1 m (Na,K) Cl	1289	0.03	0.05	115	−0.18	0.05	0.09	−0.21	0.07
Ba15	800	2	20	1.0	1 m (Na,K) Cl	1140	0.04	0.05	112	−0.20	0.04	0.10	−0.24	0.06
Ba14	800	2	40	1.0	1 m (Na,K) Cl	1145	0.07	0.03	89	−0.18	0.01	0.08	−0.25	0.03
Ba06	900	2	10	1.0	1 m (Na,K) Cl	1186	0.08	0.05	121	−0.12	0.05	0.10	−0.20	0.07
Ba07	700	2	20	1.0	1 m (Na,K) Cl	1227	0.10	0.05	69	−0.52	0.05	0.06	−0.62	0.07
Ba09	800	2	10	1.0	0.5 m (Na,K) Cl	1427	0.07	0.05	57	−0.24	0.05	0.04	−0.31	0.07
Ba10	800	2	10	1.0	1.5 m (Na,K) Cl	1291	0.05	0.05	253	−0.09	0.05	0.20	−0.14	0.07
Ba11	800	2	10	0.8	1 m (Na,K) Cl	1253	0.06	0.05	23	−0.38	0.05	0.02	−0.44	0.07
Ba12	800	2	10	1.2	1 m (Na,K) Cl	702	0.07	0.05	118	−0.09	0.05	0.17	−0.16	0.07

[a] D_{Ba} is the partitioning coefficient between fluid and melt, which is calculated from the concentration of Ba in the fluid product and that in the melt product.
[b] $\Delta^{138/134}Ba_{FLUID\text{-}MELT} = \delta^{138/134}Ba_{Fluid} - \delta^{138/134}Ba_{Melt}$, and the uncertainties (2 s.d.) are calculated by error propagation.

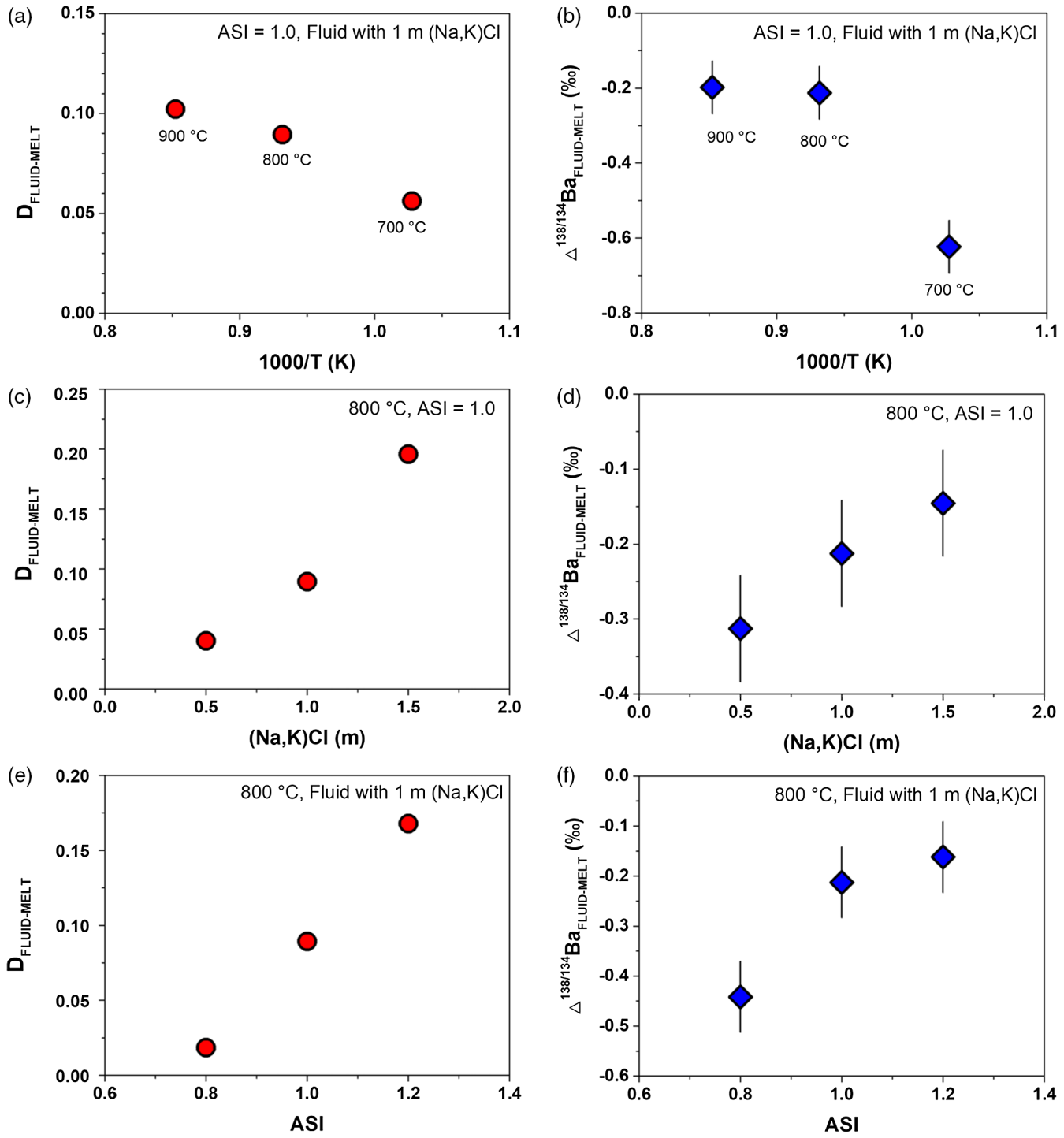

Figure 1 Partitioning coefficient ($D_{FLUID\text{-}MELT}$) and equilibrium isotope fractionation ($\Delta^{138/134}Ba_{FLUID\text{-}MELT}$) of Ba between aqueous fluid and silicate melt as a function of temperature from 700 to 900 °C **(a,b)**, salinity of the fluid **(c,d)**, and ASI of the melt **(e,f)**. Error bars in **b**, **d**, and **f** represent 2 s.d. uncertainties (see Table 1).

where T is temperature in Kelvin and Cl is the (Na, K)Cl molarity concentration of fluid. The $D_{FLUID\text{-}MELT}$ and $\Delta^{138/134}Ba_{FLUID\text{-}MELT}$ values predicted by the Eqs. 1 and 2 are consistent with the experimentally measured data (Fig. S-4), indicating that these two equations can provide reliable estimations.

Our work demonstrates for the first time that, in equilibrium conditions, aqueous fluids are enriched in light Ba isotopes compared to the coexisting silicate melts. This observation provides direct constraints on the behaviour of Ba isotopes during fluid exsolution from silicate melts. Based on the $D_{FLUID\text{-}MELT}$ and $\Delta^{138/134}Ba_{FLUID\text{-}MELT}$ obtained here (Eqs. 1 and 2), we use the Rayleigh fractionation model to simulate the Ba isotopic compositions of the exsolved aqueous fluid and residual silicate melt in natural conditions (modelling details are available in the Supplementary Information).

Figure 2 shows that the modelled $\delta^{138/134}Ba$ of the residual melt and exsolved fluid are related to the fluid fraction, temperature, ASI of the melt, and salinity of the fluid. The most obvious

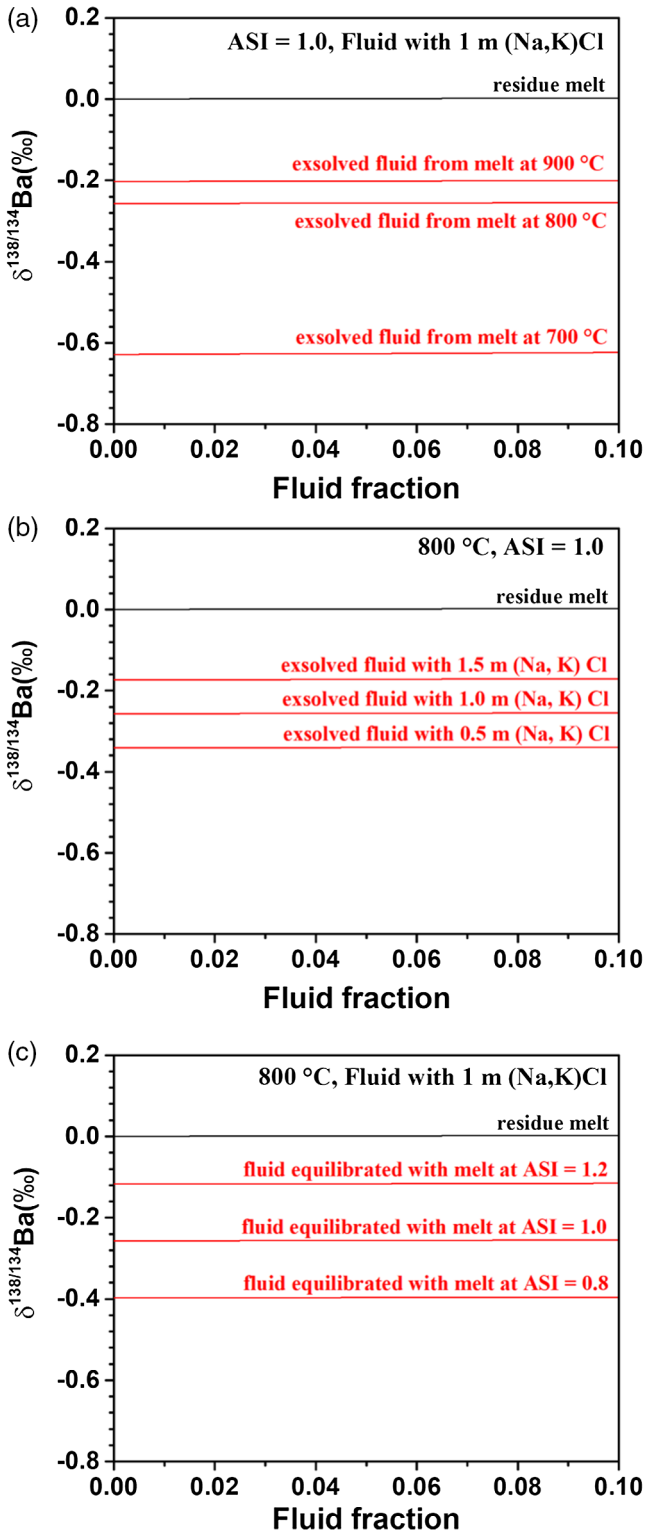

Figure 2 The modelled $\delta^{138/134}$Ba values of residue melt and exsolved fluid as a function of fluid fraction, using the Rayleigh fractionation model. The Ba isotopic composition of the initial fluid-saturated melt is set as 0 ‰, which is the average $\delta^{138/134}$Ba of the upper continental crust (Nan *et al.*, 2018). Three factors affecting the Ba isotope fractionation between the melt and fluid are considered: **(a)** temperature, **(b)** salinity of the fluid, and **(c)** ASI of the melt. Based on Eq. S-1 in the Supplementary Information, the fluid phase only removes less than 2 % of the total Ba from the hydrous magma system, even if the fluid exsolution fraction is as high as 0.1. See text for the details.

result is that $\delta^{138/134}Ba_{residual\ melt}$ is similar to that of the initial melt (set as 0 ‰ in the model), regardless of the fraction of fluid exsolution, temperature, salinity of the fluid, and ASI of the melt. The reason for the nearly unchanged Ba isotopic composition of the residual melt after fluid segregation is that Ba is incompatible in aqueous fluids relative to silicate melts (Borchert *et al.*, 2010; and this study), leading to limited fraction of Ba transferred from melts to fluids. For example, based on Eq. S-1 of the Supplementary Information, the fluid phase only removes less than 2 % of the total Ba from the hydrous melt even if the fluid exsolution fraction is as high as 0.1. On the contrary, the exsolved fluids display significantly lower $\delta^{138/134}$Ba, down to −0.63 ‰, than the residual melts (Fig. 2). The $\delta^{138/134}Ba_{exsolved\ fluid}$ depends strongly on temperature (Fig. 2a), and also on salinity of the fluid and ASI of the melt (Fig. 2b,c), *i.e.* $\delta^{138/134}Ba_{exsolved\ fluid}$ increases with increasing temperature, the (Na, K)Cl concentration and ASI.

Implications

Aqueous fluids could be derived from cooling of the hydrous crustal melts, when they rise up to the depth where the temperature decreases to the solidus. Our experimental results and models demonstrate that fluid exsolution from granitic melts cannot significantly affect the Ba isotopic composition of the residual melt (Fig. 2). Thus, our work supports the suggestion of Nan *et al.* (2018) that the light Ba isotopic compositions observed in some granites (Fig. S-1) probably result from fractional crystallisation of Ba-bearing minerals with heavy Ba isotopes rather than from fluid exsolution. More data from natural samples and experimental determination of the equilibrium Ba isotope fractionation factors between magmatic minerals and silicate melts are needed for further interpretation. In any event, the behaviour of Ba isotopes during fluid exsolution revealed in this study is essential for understanding the Ba isotopic signatures of granites.

The light Ba isotopic compositions of the aqueous fluids derived from magmas also have implications for tracing the process of extracting metal elements from magmas into fluids, which is an initial process (generally occurring at T > 600 °C) related to many kinds of magmatic-hydrothermal ore deposits. The hydrogen and oxygen isotopic data have been applied to discriminate the origin of hydrothermal fluids (*e.g.*, Sheppard, 1986), as the magmatic H_2O ($\delta D = -80 \sim -40$ ‰, $\delta^{18}O =$ ~5–10 ‰) has distinct H–O isotopic compositions from the Global Meteoric Water Line (GMWL, $\delta D = 8\delta^{18}O + 10$; Craig, 1961). However, since oxygen is a major component in both fluids and rocks, hydrothermal alteration of rocks may cause meteoric waters to have similar $\delta^{18}O$ values to those of magmatic fluids. By contrast, Ba isotopes may serve as an effective tracer of magmatic fluids because hydrothermal fluids that exsolved from melts will be enriched in light Ba isotopes (Fig. 2), whereas meteoric waters with dissolved Ba are enriched in heavy Ba isotopes (*e.g.*, $\delta^{138/134}$Ba ranging from +0.17 ‰ to +0.46 ‰; Gou *et al.*, 2020). For example, alkaline intrusions particularly have the capacity to form rare earth element and other metal deposits (*e.g.*, Verplanck *et al.*, 2014). According to Fig. 2c, the exsolved fluids from the alkaline intrusion systems (*e.g.*, ASI = 0.8) are expected to display significantly low $\delta^{138/134}$Ba (Fig. 3). In addition, pegmatites reacted with such exsolved fluids and volatiles with the potential for rare earth element mineralisation may also be characterised by light Ba isotopic compositions (Fig. 3). Therefore, Ba isotopes may be a new monitor for hydrothermal activities associated with metal mineralisation at shallow crustal levels. Such hypotheses can be tested by further measurements

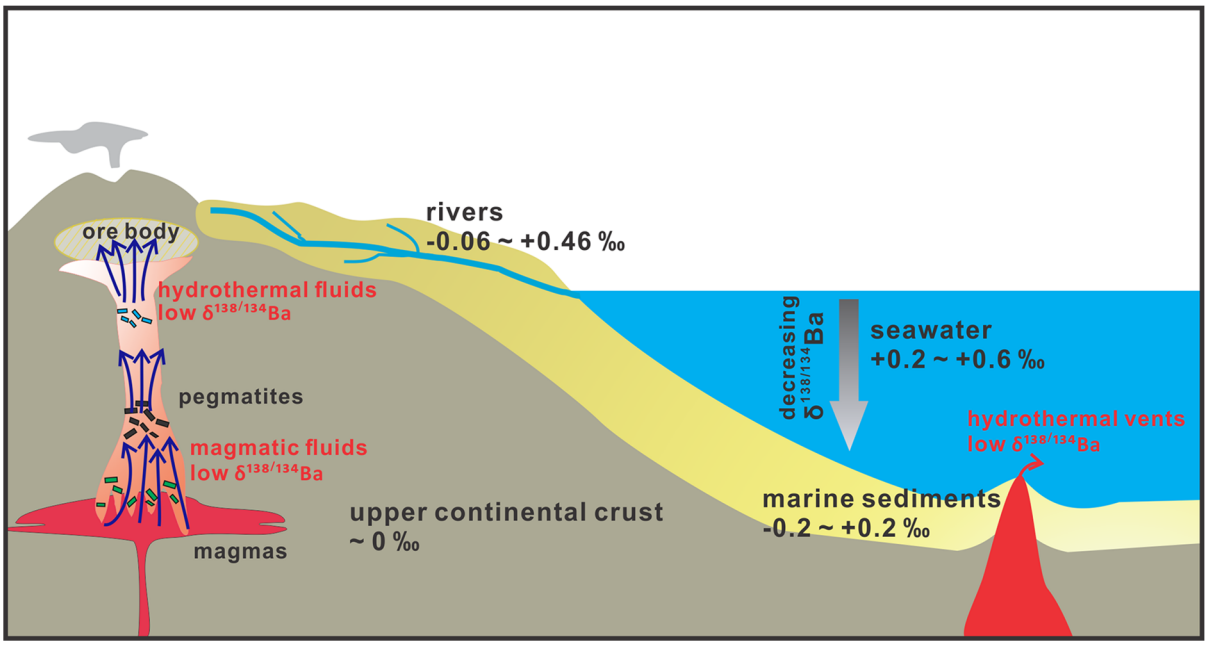

Figure 3 A schematic diagram illustrating the global $\delta^{138/134}$Ba isotopic characteristics of the upper continental crust, marine sediments, seawater and rivers as well as the relevant hydrothermal fluids and vents. The magmatic fluids, hydrothermal fluids and vents are expected to have low $\delta^{138/134}$Ba according to the negative $\Delta^{138/134}Ba_{FLUID\text{-}MELT}$ values (from –0.62 ‰ to –0.14 ‰) obtained in this study. Data sources: Horner *et al.* (2015); Cao *et al.* (2016); Bates *et al.* (2017); Hsieh and Henderson (2017); Bridgestock *et al.* (2018, 2019); Nan *et al.* (2018); Nielsen *et al.* (2018); Crockford *et al.* (2019); Gou *et al.* (2020).

of the Ba isotopic compositions of pegmatite and hydrothermal deposit samples.

Supposing that basaltic melt has a similar structure to granitic melt, the exsolved fluids from seafloor volcanoes are also expected to have low $\delta^{138/134}$Ba (<0 ‰), which will contribute to the hydrosphere (Fig. 3). The vertical ocean profiles have heterogeneous Ba isotopic compositions with the deep ocean being enriched in light Ba isotopes (~ +0.2 ‰) relative to the surface ocean (~ +0.6 ‰; Fig. 3). The light Ba isotopic compositions of the deep ocean have been suggested to result from dissolution of isotopically light barite during its sinking (*e.g.*, Horner *et al.*, 2015; Bates *et al.*, 2017; Hsieh and Henderson, 2017; Bridgestock *et al.*, 2018). Our results imply that, besides the effect of barite, fluid derived from the seafloor hydrothermal system may be another important source of isotopically light Ba to the deep ocean (Fig. 3), which should be taken into account in future studies on the global oceanic budget of Ba isotopes (the relevant Ba fluxes and isotopic compositions are shown in Fig. S-5). Collectively, our experimental results and models suggest that Ba isotopes could be a novel tracer for hydrothermal fluids in the shallow crust and at the seafloor, on the premise that more Ba isotopic data of granites, felsic intrusion-related hydrothermal deposits and seafloor hydrothermal vents will be accumulated.

Acknowledgements

We are grateful to Hui-Min Yu, Ying-Zeng Gong and Lan-Lan Tian for discussions. Heye Freymuth and an anonymous reviewer, as well as Editor Helen Williams for reviewing and improving the manuscript are thanked. This work is financially supported by the National Natural Science Foundation of China (42073004, 41803003), and the Open Research Fund of the State Key Laboratory of Ore Deposit Geochemistry of China (201805).

Editor: Helen Williams

Additional Information

Supplementary Information accompanies this letter at https://www.geochemicalperspectivesletters.org/article2036.

Cite this letter as: Guo, H., Li, W.-Y., Nan, X., Huang, F. (2020) Experimental evidence for light Ba isotopes favouring aqueous fluids over silicate melts. *Geochem. Persp. Let.* 16, 6–11.

References

Bates, S.L., Hendry, K.R., Pryer, H.V., Kinsley, C.W., Pyle, K.M., Woodward, E.M.S., Horner, T.J. (2017) Barium isotopes reveal role of ocean circulation on barium cycling in the Atlantic. *Geochimica et Cosmochimica Acta* 204, 286–299.

Borchert, M., Wilke, M., Schmidt, C., Cauzid, J., Tucoulou, R. (2010) Partitioning of Ba, La, Yb and Y between haplogranitic melts and aqueous solutions: An experimental study. *Chemical Geology* 276, 225–240.

Bridgestock, L., Hsieh, Y.-T., Porcelli, D., Homoky, W.B., Bryan, A., Henderson, G.M. (2018) Controls on the barium isotope compositions of marine sediments. *Earth and Planetary Science Letters* 481, 101–110.

Bridgestock, L., Hsieh, Y.-T., Porcelli, D., Henderson, G.M. (2019) Increased export production during recovery from the Paleocene–Eocene thermal maximum constrained by sedimentary Ba isotopes. *Earth and Planetary Science Letters* 510, 53–63.

Cao, Z., Siebert, C., Hathorne, E.C., Dai, M., Frank, M. (2016) Constraining the oceanic barium cycle with stable barium isotopes. *Earth and Planetary Science Letters* 434, 1–9.

Craig, H. (1961) Isotopic variations in meteoric waters. *Science* 133, 1702–1703.

Crockford, P.W., Wing, B.A., Paytan A., Hodgskiss, M.S.W., Mayfield, K.K., Hayles, J.A., Middleton, J.E., Ahm, A.-S.C., Johnston, D.T., Caxito, F., Uhlein, G., Halverson, G.P., Eickmann, B., Torres, M., Horner, T.J. (2019) Barium-isotopic constraints on the origin of post-Marinoan barites. *Earth and Planetary Science Letters* 519, 234–244.

Eugster, O., Tera, F., Wasserburg, G.J. (1969) Isotopic analyses of barium in meteorites and in terrestrial samples. *Journal of Geophysical Research* 74, 3897–3908.

Gou, L.-F., Jin, Z., Galy, A., Gong, Y.-Z., Nan, X.-Y., Jin, C., Wang, X.-D., Bouchez, J., Cai, H.-M., Chen, J.-B., Yu, H.-M., Huang, F. (2020) Seasonal riverine barium isotopic variation in the middle Yellow River: Sources and fractionation. *Earth and Planetary Science Letters* 531, 115990.

Guo, H., Xia, Y., Bai, R., Zhang, X., Huang, F. (2020) Experiments on Cu isotope fractionation between chlorine-bearing fluid and silicate magma: implications for fluid exsolution and porphyry Cu deposits. *National Science Review* 7, 1319–1330.

Hedenquist, J.W., Lowenstern, J.B. (1994) The role of magmas in the formation of hydrothermal ore deposits. *Nature* 370, 519.

Horner, T.J., Kinsley, C.W., Nielsen, S.G. (2015) Barium-isotopic fractionation in seawater mediated by barite cycling and oceanic circulation. *Earth and Planetary Science Letters* 430, 511–522.

Hsieh, Y.-T., Henderson, G.M. (2017) Barium stable isotopes in the global ocean: Tracer of Ba inputs and utilization. *Earth and Planetary Science Letters* 473, 269–278.

Maner, J.L., London, D. (2018) Fractionation of the isotopes of boron between granitic melt and aqueous solution at 700 °C and 800 °C (200 MPa). *Chemical Geology* 489, 16–27.

Nan, X.-Y., Yu, H.-M., Rudnick, R.L., Gaschnig, R.M., Xu, J., Li, W.-Y., Zhang, Q., Jin, Z.-D., Li, X.-H., Huang, F. (2018) Barium isotopic composition of the upper continental crust. *Geochimica et Cosmochimica Acta* 233, 33–49.

Nielsen, S.G., Horner, T.J., Pryer, H.V., Blusztajn, J., Shu, Y., Kurz, M.D., Le Roux, V. (2018) Barium isotope evidence for pervasive sediment recycling in the upper mantle. *Science Advances* 4, eaas8675.

Rudnick, R., Gao, S. (2003) Composition of the continental crust. In: Holland, H.D., Turekian, K.K. (Eds.) *Treatise on Geochemistry, Volume 3: The Crust*, Pergamon, Oxford, 1–64.

Sheppard, S.M.F. (1986) Characterization and isotopic variations in natural waters. *Reviews in Mineralogy and Geochemistry* 16, 165–183.

Sun, S.-S., McDonough, W. (1989) Chemical and isotopic systematics of oceanic basalts: implications for mantle composition and processes. *Geological Society, London, Special Publications* 42, 313–345.

Tivey, M.K. (2007) Generation of seafloor hydrothermal vent fluids and associated mineral deposits. *Oceanography* 20, 50–65.

Telus, M., Dauphas, N., Moynier, F., Tissot, F.L.H., Teng, F.-Z., Nabelek, P.I., Craddock, P.R., Groat, L.A. (2012) Iron, zinc, magnesium and uranium isotopic fractionation during continental crust differentiation: The tale from migmatites, granitoids, and pegmatites. *Geochimica et Cosmochimica Acta* 97, 247–265.

Verplanck, P.L., Van Gosen, B.S., Seal, R.R., McCafferty, A.E. (2014) A deposit model for carbonatite and peralkaline intrusion-related rare earth element deposits. *U.S. Geological Survey Scientific Investigations Report*, 2010-5070-J.

Workman, R.K., Hart, S.R. (2005) Major and trace element composition of the depleted MORB mantle (DMM). *Earth and Planetary Science Letters* 231, 53–72.

Geochemical Perspectives Letters

Experimental evidence for light Ba isotopes favouring aqueous fluids over silicate melts

H. Guo, W.-Y. Li, X. Nan, F. Huang

Supplementary Information

The Supplementary Information includes:

- Starting Materials and Encapsulation
- High Temperature and Pressure Experiments
- Run Product Separation and Dissolution
- Barium Concentration Analyses
- Barium Isotope Analyses
- Rayleigh Fractionation Model
- Figures S-1 to S-5
- Supplementary Information References

Starting Materials and Encapsulation

The starting haplogranitic glasses were prepared from stoichiometric mixtures of analytical grade SiO_2, $Al(OH)_3$, Na_2CO_3, and K_2CO_3. The haplogranitic composition corresponds to the 2 kbar haplogranite eutectic melt composition ($Qz_{35}Ab_{40}Or_{25}$; Johannes and Holtz, 1996), and the alumina saturation index (ASI) was set to be 0.8, 1.0 and 1.2 by varying the amounts of $Al(OH)_3$, Na_2CO_3, and K_2CO_3 at a constant Na/K-ratio. The mixtures were dehydrated and decarbonated in a platinum crucible by heating from room temperature to 1100 °C at a rate of 100 °C /h and holding at 1100 °C for a further 12 h in a muffle furnace. The recovered samples were ground to fine powders in an agate mortar until they were homogenised and free of gas bubbles, then melted at 1600 °C for 2 h in a platinum crucible and quenched in distilled water. Part of these glass powders were then doped with ~1000 ppm Ba by mixing them thoroughly with $Ba(NO_3)_2$. The Ba-doped glass powders were heated at 1100 °C for 12 h to remove nitrogen

($Ba(NO_3)_2$ was decomposed to BaO and NO_2 at this temperature) and then remelted at 1600 °C in a platinum crucible for 2 h in the furnace. Aqueous fluids with the (Na, K)Cl (Na:K = 1:1 in moles) concentration of 0.5, 1 and 1.5 mol/L were prepared with deionised H_2O, analytical grade NaCl and KCl.

All experiments were conducted in Bayerisches Geoinstitut, University of Bayreuth. Silicate glass powders and the nearly similar amount of aqueous fluids (~100 mg) were loaded into Au capsules with 4.3 mm O.D. (outer diameter), 4.0 mm I.D. (inner diameter) and 2.5 mm length (Fig. S-2a). Capsules were welded and then put in an oven at 110 °C to check potential leaks, and the capsules with obvious weight changes were discarded.

High Temperature and Pressure Experiments

The capsules were then loaded into vertical rapid-quench cold-seal pressure vessels made of Inconel 713LC super alloy using water as the pressure medium, with the setup similar to that described in Matthews *et al.* (2003). Temperatures were measured with NiCr-Ni (K-type) thermocouples in an external borehole of the vessels. The uncertainties of the temperature and pressure are smaller than 5 °C and 30 bar, respectively. Oxygen fugacity was not specifically controlled in the vessels, but it should be 0.5 to 1 log unit above the Ni-NiO buffer as suggested by the reaction of water with the autoclave material (Keppler, 2010). All experiments were run at 700 to 900 °C and 200 MPa for 10 to 40 days (Table 1). The samples were quenched by dropping the external magnet to force the sample to fall into the water-cooled zone within a few seconds.

Run Product Separation and Dissolution

The capsules were recovered and weighed again to check for potential leaks during the experiments. Those without obvious weight changes were then cleaned, cooled by liquid-N_2, and then punctured with a steel needle. After the solution was withdrawn as much as possible with a micropipette, the capsules were opened and boiled in deionised water for 30 minutes. After that, they were further rinsed several times with deionized water. All solutions obtained during these operations were added together with the solution phase withdrew from the experiment. This procedure is similar to the treatment of Keppler and Wyllie (1991) in re-dissolving materials precipitated from the fluid during quenching. The capsule and recovered glass samples were dried at 130 °C in the oven for at least 2 h. Then, the Au capsule material and glass were weighed to determine the actual fluid weight after quenching by subtraction. Previous studies showed that such a method works well under relatively low-pressure experiments (<1 GPa; Borchert *et al.*, 2010; Keppler, 2017), which is suitable for the experiments conducted at 200 MPa in this study.

The solution extracted from each run product was transferred directly into a pre-cleaned screw-top Teflon beaker, and then evaporated to dryness at 100 ºC on a hot plate. The dried residue was dissolved in 2 mL concentrated HCl (all of the acids used in this study throughout the dissolution and purification processes were produced by double sub-boiling distillation). The solution was divided into two parts and processed as follows: (1) 0.1 mL of the solution was transferred into a pre-cleaned Teflon tube, and then diluted to 3 mL for Ba concentration analyses; (2) the other 1.9 mL

of the solution was evaporated to dryness, and then diluted with 3 mol/L HCl to achieve the desired Ba concentration of ~2 ppm, in preparation for column chemistry.

The melt-quenched glass in each run product was firstly ground to fine powders in an agate mortar, in order to crush fluid inclusions that were possibly trapped in the glass (Fig. S-2b). Then, the powder was transferred into a pre-cleaned Teflon tube, and rinsed with ~70 ºC ultra-pure water (18.2 MΩ.cm) for three times to remove the concomitant fluid released from fluid inclusions during crushing. Finally, the powder was dried at 105 ºC in an oven, weighed into a pre-cleaned screw-top Teflon beaker, dissolved in a combination of concentrated HF-HNO_3-HCl, and evaporated to dryness on a hot plate. The following procedures for the dried residue were the same as those described above for the fluid phase extracted from the run products.

Barium Concentration Analyses

As described above, a small fraction of each sample solution was diluted to ~1% HCl for Ba concentration analyses. The analyses were conducted using a Perkin-Elmer ELAN DCR-II inductively coupled plasma mass spectrometer (ICP-MS) at the CAS Key Laboratory of Crust-Mantle Materials and Environments, University of Science and Technology of China (USTC), Hefei. The procedures were described in Hou and Wang (2007). The relative standard deviation (RSD) of Ba concentration is better than 5 %.

Barium Isotope Analyses

Barium isotope analyses were performed at the CAS Key Laboratory of Crust-Mantle Materials and Environments, USTC, Hefei. All chemical procedures were carried out in an ISO-class 6 clean laboratory. The chemical purification of Ba was achieved by cation exchange chromatography with pre-cleaned resin (Bio-Rad 200-400 mesh AG50W-X12), following established procedures (Nan *et al.*, 2015, 2018). Sample solutions containing ~2 μg Ba were loaded onto the resin. The Ba recoveries through column chemistry, based on analyses of Ba concentration in the elution collected before and after the Ba cut, were >99%. The procedural blank was 2 ng Ba.

Barium isotope measurements were carried out on a Neptune Plus multi-collector inductively coupled plasma mass spectrometer (MC-ICP-MS), and a double-spike (^{135}Ba-^{136}Ba) technique was used to correct for instrumental mass bias. The "dry" plasma conditions (Aridus II desolvating nebuliser) were used to increase sensitivity. Barium isotope analyses were conducted in a low-resolution mode, with ^{134}Ba, ^{135}Ba, ^{136}Ba, ^{137}Ba and ^{138}Ba collected simultaneously by the L2, L1, C, H1 and H2 Faraday cups, respectively. ^{131}Xe and ^{140}Ce were also collected by the L4 and H3 Faraday cups to correct the effects of isobaric interferences from Xe and Ce. The background signals for ^{138}Ba (<0.03 V) were negligible relative to the sample signals (~30 V of the measured solutions with the Ba concentration of ~100 ppb).

The Ba isotopic data are reported in δ-notation in per mil relative to NIST SRM3104a, i.e., $\delta^{138/134}$Ba =

$[(^{138}Ba/^{134}Ba)_{sample}/(^{138}Ba/^{134}Ba)_{SRM3104a} - 1] \times 1000$. Based on replicate analyses of two in-house reference solutions USTC-Ba and ICPUS-Ba during this study, the external precision is better than 0.05‰ on $\delta^{138/134}$Ba (2SD). To monitor the accuracy, two reference materials G-2 and GSP-2 were processed through the column chemistry with samples. The $\delta^{138/134}$Ba values of granite G-2 (+0.01 ± 0.04 ‰, 2SD, *n* = 4) and granodiorite GSP-2 (-0.04 ± 0.05 ‰, 2SD, *n* = 6) obtained in this study agree well with previously published values within analytical uncertainties (+0.03 ± 0.04 ‰ and +0.04 ± 0.04 ‰ of G-2, and +0.02 ± 0.05‰ and 0 ± 0.04 ‰ of GSP-2; Nan *et al*., 2015, 2018; van Zuilen, 2016). For comparison, the published $\delta^{137/134}$Ba values have been converted to $\delta^{138/134}$Ba values by assuming mass-dependent fractionation following $\delta^{138/134}Ba \approx 1.33 \times \delta^{137/134}Ba$ (Horner *et al*., 2015).

Rayleigh Fractionation Model

The fraction of Ba in the residual melt (*f*) after fluid exsolution from melt can be defined as a function of the fraction of fluid exsolution (F) and $D_{FLUID\text{-}MELT}$ in Eq. S-1.

$$f = (1 - F)^{D_{FLUID-MELT}} \qquad \text{Eq. S-1}$$

The equilibrium Ba isotope fractionation factor (α) between fluid and melt is calculated based on the $\Delta^{138/134}Ba_{FLUID\text{-}MELT}$ described in Eq. 2.

$$\alpha \approx 1 + \frac{\triangle^{138/134}Ba_{FLUID-MELT}}{1000} \qquad \text{Eq. S-2}$$

With the *f* and α values calculated above, the Ba isotopic composition of the cumulative exsolved fluid and residual melt can be described by Eq. S-3 and Eq. S-4, respectively:

$$\delta^{138/134}Ba_{\text{exsolved } fluid} = \left(\delta^{138/134}Ba_{initial} + 1000\right)(f^{\alpha} - 1)/(f - 1) - 1000 \qquad \text{Eq. S-3}$$

$$\delta^{138/134}Ba_{residual\ melt} = (\delta^{138/134}Ba_{initial} + 1000)\, f^{(\alpha-1)} - 1000 \qquad \text{Eq. S-4}$$

where $\delta^{138/134}Ba_{initial}$ is the Ba isotopic composition of the initial fluid-saturated melt in nature. Supposing that the $\delta^{138/134}Ba_{initial}$ value equals to the average Ba isotopic composition of the upper continental crust (*i.e.* 0 ‰; Nan *et al*., 2018), the $\delta^{138/134}Ba_{\text{exsolved } fluid}$ and $\delta^{138/134}Ba_{\text{residual } melt}$ can be modeled using Eqs. 1, 2 and S-1 to S-4. Since the fluid content in silicate melts is usually less than 10 wt. % (*e.g*., Edmonds and Woods, 2018), up to 10 % fluid fraction (*i.e.* F = 0.1) is considered in the model.

Supplementary Figures

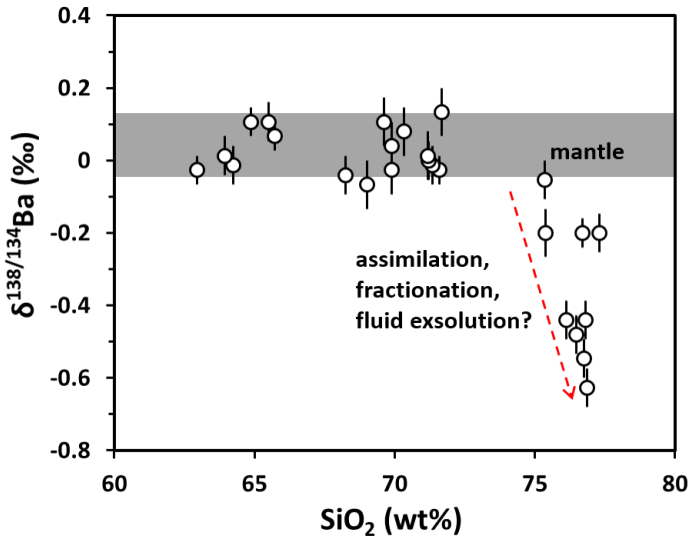

Figure S-1 $\delta^{138/134}$Ba vs. SiO_2 content of granite samples reported in Nan *et al.* (2018). Error bars represent 2SD uncertainties. The gray area represents the estimated average $\delta^{138/134}$Ba of the mantle (Li *et al.*, 2020). The $\delta^{137/134}$Ba reported in the literature has been converted to $\delta^{138/134}$Ba assuming mass-dependent fractionation following $\delta^{138/134}\text{Ba} \approx 1.33 \times \delta^{137/134}\text{Ba}$ (Horner *et al.*, 2015).

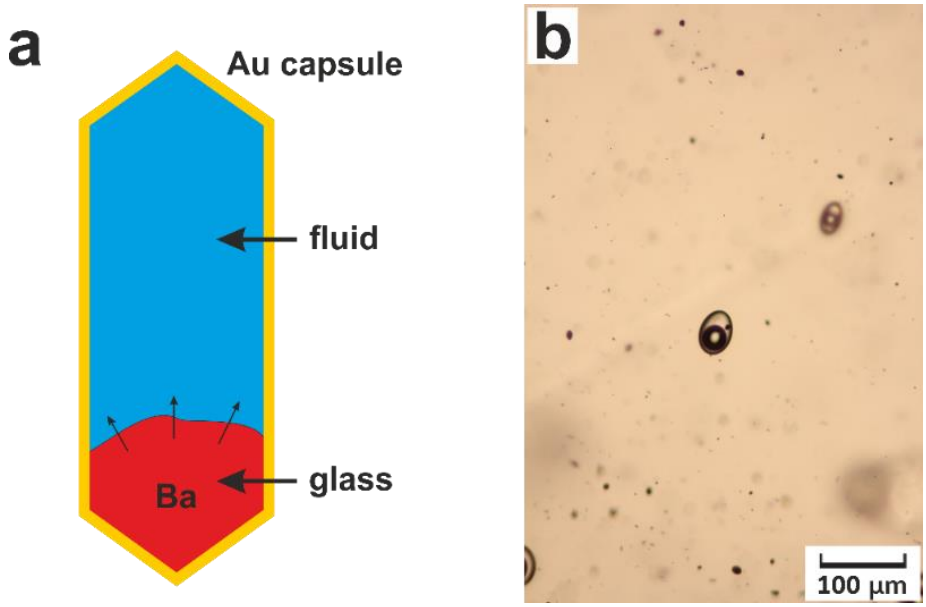

Figure S-2 (a) Experimental design with Ba-doped haplogranitic glass and (Na, K)Cl bearing fluid starting materials in a gold capsule. The outer diameter of the Au capsule is 4.3 mm. **(b)** A typical run product showing fluid inclusions in quenched glass (Run No. Ba05).

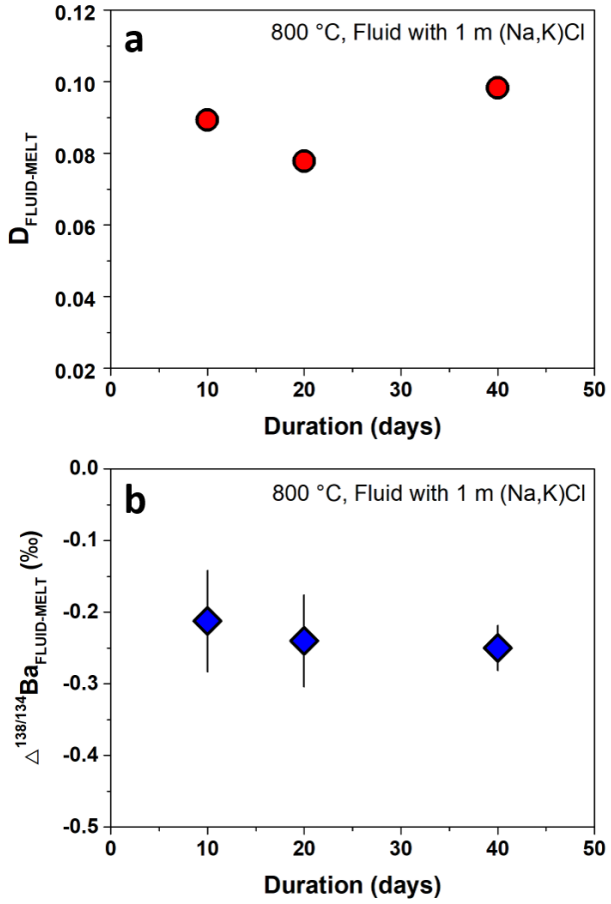

Figure S-3 Partitioning coefficient ($D_{FLUID-MELT}$) and isotope fractionation ($\Delta^{138/134}Ba_{FLUID-MELT}$) of Ba between aqueous fluid and silicate melt as a function of run durations (10, 20 and 40 days). Error bars in Figure S-3b represent 2SD uncertainties (see Table 1).

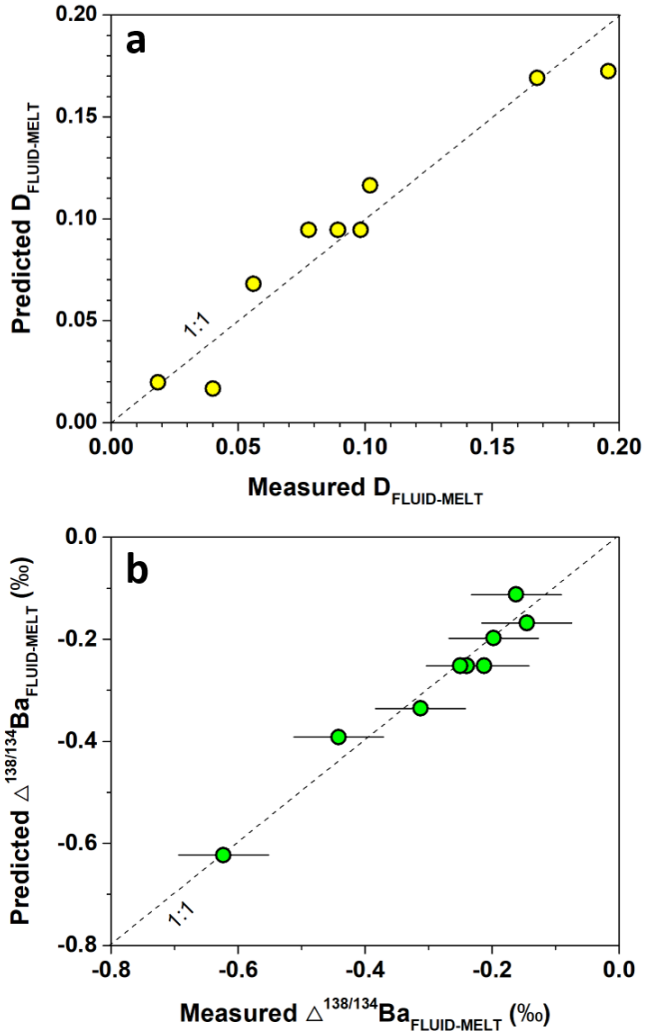

Figure S-4 Comparison between the experimentally measured data (Table 1) and predicted results based on Eqs. 1 and 2 for **(a)** partitioning coefficient of Ba ($D_{FLUID-MELT}$), and **(b)** equilibrium isotope fractionation of Ba ($\Delta^{138/134}Ba_{FLUID-MELT}$) between aqueous fluid and silicate melt.

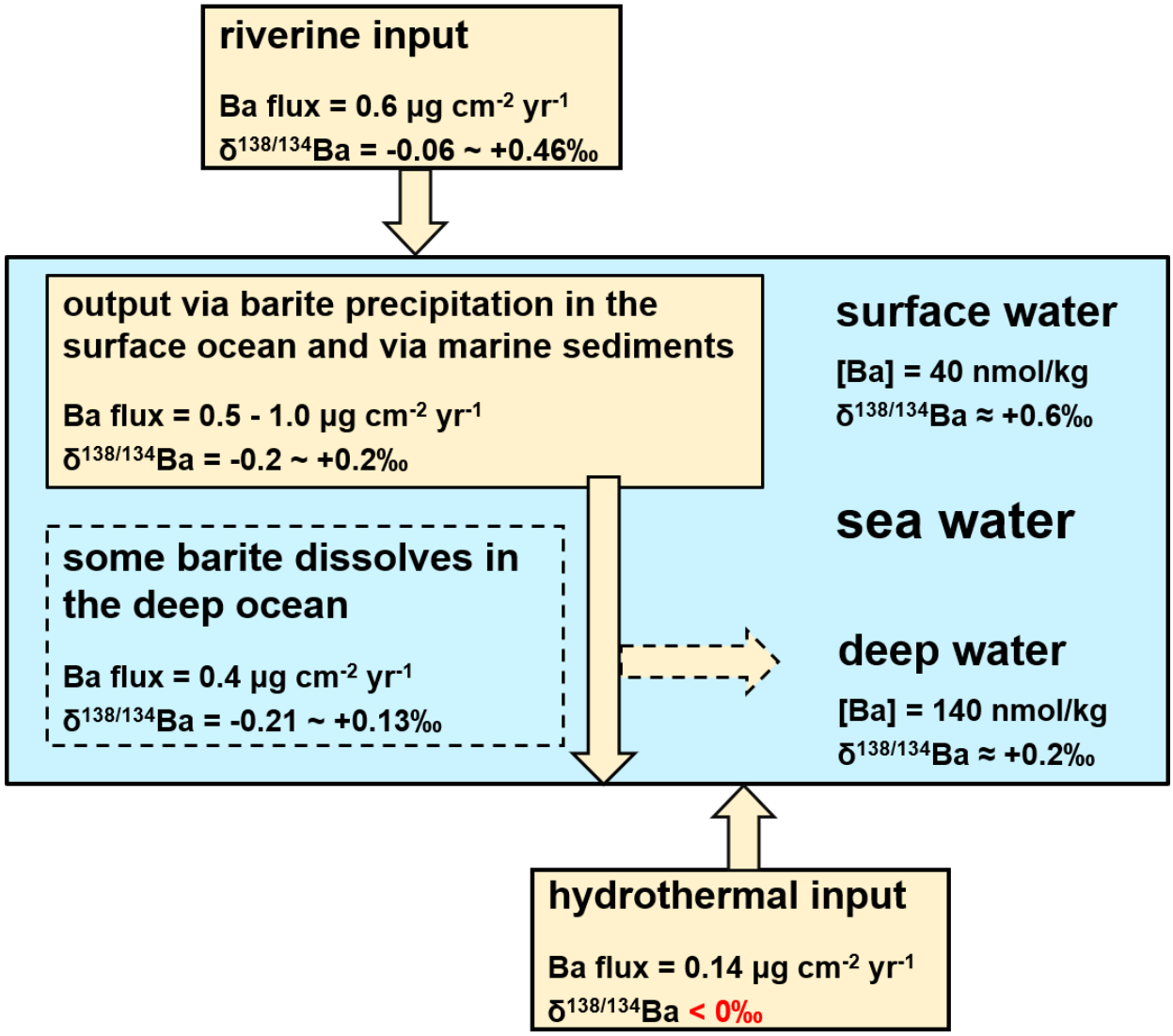

Figure S-5 A preliminary box model for the cycle of Ba and Ba isotopes in the ocean. Oceanic crust alteration is ignored in this model as the net alteration flux of Ba is insignificant (*e.g.*, Kelley *et al.*, 2003). The Ba fluxes of the riverine input, hydrothermal input, precipitation output, and barite dissolution, as well as the mean Ba concentrations of surface and deep sea water are from Dehairs *et al.* (1980) and Paytan and Kastner (1996). The $\delta^{138/134}$Ba of rivers are from Cao *et al.* (2016) and Gou *et al.* (2020). The $\delta^{138/134}$Ba of sea water are from Horner *et al.* (2015), Bates *et al.* (2017), Hsieh and Henderson (2017), and Bridgestock *et al.* (2018). The $\delta^{138/134}$Ba of barite and marine sediments are from Bridgestock *et al.* (2018, 2019), Nielsen *et al.* (2018), and Crockford *et al.* (2019).

Supplementary Information References

Bates, S.L., Hendry, K.R., Pryer, H.V., Kinsley, C.W., Pyle, K.M., Woodward, E.M.S., Horner, T.J. (2017) Barium isotopes reveal role of ocean circulation on barium cycling in the Atlantic. *Geochimica et Cosmochimica Acta* 204, 286-299.

Borchert, M., Wilke, M., Schmidt, C., Cauzid, J., Tucoulou, R. (2010) Partitioning of Ba, La, Yb and Y between haplogranitic melts and aqueous solutions: An experimental study. *Chemical Geology* 276, 225-240.

Bridgestock, L., Hsieh, Y.-T., Porcelli, D., Homoky, W.B., Bryan, A., Henderson G.M. (2018) Controls on the barium isotope compositions of marine sediments. *Earth and Planetary Science Letters* 481, 101-110.

Bridgestock, L., Hsieh, Y.-T., Porcelli, D., Henderson, G.M. (2019) Increased export production during recovery from the Paleocene–Eocene thermal maximum constrained by sedimentary Ba isotopes. *Earth and Planetary Science Letters* 510, 53-63.

Cao, Z., Siebert, C., Hathorne, E.C., Dai, M., Frank, M. (2016) Constraining the oceanic barium cycle with stable barium isotopes. *Earth and Planetary Science Letters* 434, 1-9.

Crockford, P.W., Wing, B.A., Paytan A., Hodgskiss, M.S.W., Mayfield, K.K., Hayles, J.A., Middleton, J.E., Ahm, A.-S.C., Johnston, D.T., Caxito, F., Uhlein, G., Halverson, G.P., Eickmann, B., Torres, M., Horner, T.J.. (2019) Barium-isotopic constraints on the origin of post-Marinoan barites. *Earth and Planetary Science Letters* 519, 234-244.

Dehairs, F., Chesselet, R., Jedwab, J. (1980) Discrete suspended particles of barite and the barium cycle in the open ocean. *Earth Planet. Sci. Lett.* 49, 528-550.

Edmonds, M., Woods, A.W. (2018) Exsolved volatiles in magma reservoirs. *Journal of Volcanology and Geothermal Research* 368, 13-30.

Gou, L.-F., Jin, Z., Galy, A., Gong, Y.-Z., Nan, X.-Y., Jin, C., Wang, X.-D., Bouchez, J., Cai, H.-M., Chen, J.-B., Yu, H.-M., Huang, F. (2020) Seasonal riverine barium isotopic variation in the middle Yellow River: Sources and fractionation. *Earth and Planetary Science Letters* 531, 115990.

Horner, T.J., Kinsley, C.W., Nielsen, S.G. (2015) Barium-isotopic fractionation in seawater mediated by barite cycling and oceanic circulation. *Earth and Planetary Science Letters* 430, 511-522.

Hou, Z., Wang, C. (2007) Determination of 35 trace elements in geological samples by inductively coupled plasma mass spectrometry. *Journal of University of Science and Technology of China* 37, 940-944.

Hsieh, Y.-T., Henderson, G.M. (2017) Barium stable isotopes in the global ocean: Tracer of Ba inputs and utilization. *Earth and Planetary Science Letters* 473, 269-278.

Johannes, W., Holtz, F. (1996) Petrogenesis and Experimental Petrology of Granitic Rocks, Springer, Berlin, 335 p.

Kelley, K.A., Plank, T., Ludden, J., Staudigel, H. (2003) Composition of altered oceanic crust as ODP Sites 801 and 1149. *Geochemistry Geophysics Geosystems* 4, 8910.

Keppler, H. (2010) The distribution of sulfur between haplogranitic melts and aqueous fluids. *Geochimica et Cosmochimica Acta* 74, 645-660.

Keppler, H. (2017), Fluids and trace element transport in subduction zones, *American Mineralogist* 102, 5-20.

Keppler, H., Wyllie, P.J. (1991) Partitioning of Cu, Sn, Mo, W, U, and Th between melt and aqueous fluid in the systems haplogranite-H_2O-HCl and haplogranite-H_2O-HF. *Contributions to Mineralogy and Petrology* 109, 139-150.

Li, W.-Y., Yu, H.-M., Xu, J., Halama, R., Bell, K., Nan, X.-Y., Huang, F. (2020) Barium isotopic composition of the mantle: Constraints from carbonatites. *Geochimica et Cosmochimica Acta* 278, 235-243.

Matthews, W., Linnen, R.L., Guo, Q. (2003) A filler-rod technique for controlling redox conditions in cold-seal pressure vessels. *American Mineralogist* 88, 701-707.

Nan, X., Wu, F., Zhang, Z., Hou, Z., Huang, F., Yu, H. (2015) High-precision barium isotope measurements by MC-ICP-MS. *Journal of Analytical Atomic Spectrometry* 30, 2307-2315.

Nan, X.-Y., Yu, H.-M., Rudnick, R.L., Gaschnig, R.M., Xu, J., Li, W.-Y., Zhang, Q., Jin, Z.-D., Li, X.-H., Huang, F. (2018) Barium isotopic composition of the upper continental crust. *Geochimica et Cosmochimica Acta* 233, 33-49.

Paytan, A., Kastner, M. (1996) Benthic Ba fluxes in the central Equatorial Pacific, implications for the oceanic Ba cycle. *Earth and Planetary Science Letters* 142, 439-450.

van Zuilen, K., Nägler, T.F., Bullen, T.D. (2016) Barium isotopic compositions of geological reference materials. *Geostandards and Geoanalytical Research* 40, 543-558.

Wallace, P.J. (2005) Volatiles in subduction zone magmas: concentrations and fluxes based on melt inclusion and volcanic gas data. *Journal of Volcanology and Geothermal Research* 140, 217-240.